Geochemistry Geophysics Geosystems G3

Article
Volume 13, Number 1
29 November 2012
Q0AF06, doi:10.1029/2012GC004122
ISSN: 1525-2027

Published by AGU and the Geochemical Society

New insights on the offshore extension of the Great Sumatran fault, NW Sumatra, from marine geophysical studies

D. Ghosal, S. C. Singh, A. P. S. Chauhan, and N. D. Hananto

Laboratoire de Géosciences Marines, Institut de Physique du Globe de Paris, 1 rue Jussieu, CEDEX 05, FR-75238 Paris, France (ghosal@ipgp.fr)

[1] Over the last 20 years, the Great Sumatran Fault (GSF) has been studied on land, but we have very little information about its offshore extension NW of Sumatra and its link with the West Andaman Fault to the north. The problem is further complicated by its vicinity to the volcanic arc. Here we present detailed analyses of the offshore extension of the GSF based on recently acquired high-resolution bathymetry, multichannel seismic reflection data and some old single channel seismic reflection data. Our findings demonstrate that the branches of the GSF near Banda Aceh proceed further northwestward producing two 15–20 km wide adjacent basins. The southwestern transpressional Breueh basin is 1–2 km deep and has a flower structure with a push-up ridge in the center, suggesting the presence of an active strike-slip fault. The presence of strike-slip earthquakes beneath this basin further suggests that one active branch of the GSF passes through this basin. The northeastern transtensional Weh basin is up to 3.4 km deep and the absence of recent sediments on the basin floor suggests that the basin is very young. The presence of a chain of volcanoes in the center of the basin suggests that the Sumatran volcanic arc passes through this basin. The anomalous depth of the Weh basin might be a site of early back-arc spreading or may have resulted from pull-apart extension. We examine all these new observations in the light of plate motion, local deformation and possible seismic risk.

Components: 11,100 words, 9 figures.

Keywords: Great Sumatra Fault; back-arc spreading; pull-apart basin; strike-slip fault; volcanic arc.

Index Terms: 0910 Exploration Geophysics: Data processing; 0935 Exploration Geophysics: Seismic methods (3025, 7294); 0999 Exploration Geophysics: General or miscellaneous.

Received 24 February 2012; **Revised** 20 September 2012; **Accepted** 17 October 2012; **Published** 29 November 2012.

Ghosal, D., S. C. Singh, A. P. S. Chauhan, and N. D. Hananto (2012), New insights on the offshore extension of the Great Sumatran fault, NW Sumatra, from marine geophysical studies, *Geochem. Geophys. Geosyst.*, *13*, Q0AF06, doi:10.1029/2012GC004122.

Theme: Assessing Magmatic, Neovolcanic, Hydrothermal, and Biological Processes along Intra-Oceanic Arcs and Back-Arcs

1. Introduction

[2] In the Sumatra subduction system, the oblique convergence of the Indo-Australian oceanic plate beneath the Eurasian plate is partitioned into a trench normal thrust component and a trench sub-parallel shear component within the overriding continental lithosphere [*Fitch*, 1972; *McCaffrey*, 1992]. The

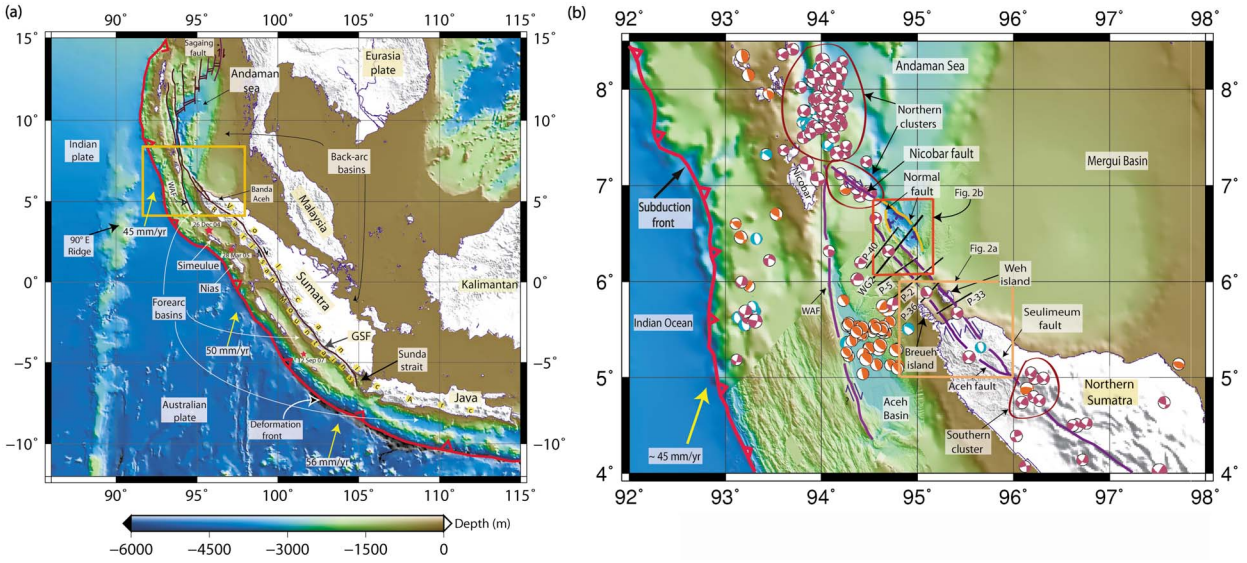

Figure 1. (a) The tectonic map of Sumatra subduction zone. GSF: Great Sumatran Fault, WAF: West Andaman Fault. The orange rectangle marks region shown in Figure 1b. (b) Bathymetry data were compiled from the French surveys [*Singh et al.*, 2008] with GEBCO data set in background. Black lines indicate seismic profiles (P-40, P-5, P-2, P-36, P-32, WG2) discussed in the paper. Earthquake CMT solutions are from Harvard catalog; locations are from the EHB catalog. Blue: Normal events, Red: Strike-slip events and Orange: Thrust events. Brown contours indicate area with strong seismic activities discussed in the paper. Orange rectangle indicates the bathymetry shown in Figure 2. This figure is also shown without interpretation in Figure S1.

trench sub-parallel shear component is taken up by a dextral type strike-slip fault: the Great Sumatra Fault (GSF). Nearly 1900-km long [*Sieh and Natawidjaja*, 2000], the GSF is elongated along the entire length of Sumatra mainland from the Sunda strait in the southeast to Banda Aceh in the northwest mimicking the trend of the Sunda plate margin and finally joins with the West Andaman Fault (WAF), a series of transform faults and spreading centers in the Andaman Sea (Figure 1a). From south to north along the western margin of Sumatra, the GSF has not remained intact structurally; instead it has split into several segments producing many dilatational and contractional step-overs [*Newcomb and McCann*, 1987; *Sieh and Natawidjaja*, 2000]. *Sieh and Natawidjaja* [2000] discovered more than a dozen of such step-overs in mainland Sumatra and suggested that most of them might have acted as structural barriers that constrain both the magnitudes and rupture dimensions of historic earthquakes. An example of structural segmentation of the GSF is observed in northern Sumatra near Banda Aceh at 4.93°N, 95.55°E where the GSF bifurcates (Figure 1b) into two strands: the Aceh fault and the Seulimeum fault, and continues offshore northwest of Sumatra. *Sieh and Natawidjaja* [2000] provide a very detailed and complete neotectonic map of the GSF onshore Sumatra, but we have very limited knowledge of the offshore extension of its branches. The absence of high-resolution geophysical offshore data sets has restricted our understanding of seismic and tsunami risks in this region.

[3] The oblique convergence of the subducting Indo-Australian plate triggers numerous earthquakes of variable magnitudes all along the Sumatra subduction zone. In just the last decade alone there have been three great megathrust earthquakes along the western coast of Sumatra. The recent seismicity started on the 26th December 2004 with a 9.2 magnitude earthquake [*Subarya et al.*, 2006; *Chlieh et al.*, 2007] that ruptured almost 1300 km of the plate boundary starting from the north of Simeulue Island and extending to the northern Andaman Island, leading to a disastrous tsunami that resulted in the loss of >230,000 lives and extensive loss of property and infrastructure. Two more megathrust earthquakes of magnitude >8.4 [*Briggs et al.*, 2006; *Konca et al.*, 2008; *Sieh et al.*, 2008] occurred further south of Simeulue Island breaking different blocks of the locked plate boundary, but no major earthquakes have occurred along the GSF. Furthermore, north of the Sumatra mainland earthquakes of magnitude

M_w >7.9 have not been observed for the last 100 years [*McCloskey et al.*, 2005]. Although some local land deformation has been observed in the Banda Aceh region, it is confined to the localized movement of the existing fault systems [*Soetadi and Soekarman*, 1964; *Sieh and Natawidjaja*, 2000]. The scarcity of seismicity over the northern segment of Sumatra is of serious concern because several sections of the GSF contain seismic gaps that could rupture easily by "gap filling" earthquake events [*Newcomb and McCann*, 1987]. In fact, soon after the 2004 megathrust earthquake, *McCloskey et al.* [2005] suggested that this earthquake has induced stress on the northern portion of the GSF making it a potential site of a large earthquake. Therefore, it is important to study the offshore extension of the GSF.

[4] The Sumatra subduction system contains a vast back-arc and a conspicuous volcanic arc. Rifting and basin formation started in Sumatra during the Palaeogene period [*Clure*, 2005]. Several hypotheses [*Karig*, 1971; *Sleep and Toksoz*, 1971; *Dewey*, 1980; *Carlson et al.*, 1983; *Jarrard*, 1986; *Scholz and Campos*, 1995] have been proposed to explain the mechanism of large back-arc basin formation, but these explanations do not fully describe the mechanics necessary for smaller arc related basin formation. The area offshore of northwestern Sumatra contains a few smaller basins that are associated with the arc, and whose mechanism of formation remains to be explained. The interference of the GSF with a chain of volcanoes within these basins complicates this effort. Although the evolution of the volcanic arc on mainland Sumatra has been studied rigorously [*van Bemmelen*, 1949; *Katili*, 1975; *Hamilton*, 1979; *Cameron et al.*, 1980; *Rock et al.*, 1982; *Macpherson and Hall*, 1999; *Crow*, 2005; *Gasparon*, 2005], the features of the volcanic structures offshore of NW Sumatra are poorly studied due to the dearth of appropriate geophysical data sets.

[5] In this paper, we present results from recently acquired bathymetry and wide-angle seismic reflection and refraction data between 4°–8.5°N and 92°–98°E (Figure 1b) between the India-Indonesia border and Banda Aceh. In order to determine the seismic velocity of the subsurface, we have carried out a high-resolution tomographic analysis of the refraction-seismic data that were downward continued to the seafloor. We use these velocities to depth migrate the seismic reflection data. We also use five historical single channel seismic profiles crossing the northwestern segment of the GSF that were acquired in 1992 [*Malod and Kamal*, 1996]. Bathymetric data allow us to identify geomorphic features such as basins, volcanoes, and faults, whereas seismic profiles define the precise locations of the offshore extension of the Aceh fault and local deformation present in some of the basins. Focal mechanisms of earthquake events from the Harvard CMT solution catalog (http://www.seismology.harvard.edu) and locations of these events from the EHB catalog (http://www.isc.ac.uk/ehbbulletin/search/catalogue/) are used to determine active zones and the nature of the faulting. These results are used to shed light upon the seismic risk in the region.

2. Background

2.1. Formation of the GSF

[6] The Sumatra subduction zone extending from Sumatra to Timor has not been fixed since its origin, but its position has shifted over geological time periods [*Katili*, 1975]. The Sunda arc first started rotating clockwise at 59 Ma (early Tertiary) forming Sagaing Fault in Burma, which was followed by the formation of the West Andaman Fault and the Mentawai Fault in the south [*Curray*, 2005]. Around 15 Ma (early Miocene) the West Andaman Fault and the Mentawai Fault stepped eastward to form the Sumatra Fault system and the Batee Fault. This stepping process continued until 4 Ma. From 4 Ma onwards the GSF started to bifurcate into Aceh Fault and Seulimeum Fault [*Curray*, 2005].

2.2. Volcanism in Sumatra

[7] Geochemical data suggest that volcanism in Sumatra initiated during the Pre-Tertiary period [*Rock et al.*, 1982] but its intensity increased rapidly during the Tertiary period. In the Paleocene, a volcanic arc was active along the southern margin of the Sunda Microplate [*Crow*, 2005] and at the same time another inner arc was situated where the North Sumatra back-arc basin was built in recent time. In the late Oligocene period all the Sumatran back-arc basins caused fault inversions [*Crow*, 2005] followed by uplifting of the volcanic arc and enormous eruption of lava and ash took place along a linear arc, parallel to the west coast of Sumatra. Neogene volcanism in Sumatra was mostly governed by the subduction rollback mechanism [*van Bemmelen*, 1949; *Macpherson and Hall*, 1999]. Quaternary volcanoes are mostly found in northern Sumatra and are mainly composed of calc-alkaline basalts, andesites and dacites [*Rock et al.*, 1982]. Originally these rocks are related to the southward

subduction of the Andaman sea micro-oceanic crust [*Rock et al.*, 1982].

2.3. Neotectonic Settings of Sumatra

[8] At the present time mainland Sumatra is the southwestern most landmass of the Sundaland block where the Indo-Australian oceanic plate obliquely subducts below it. It is characterized by sedimentary back-arc basins in the east and ~100 km wide Barisan mountains in the west, and includes the GSF and the volcanic arc along its western margin [*McCaffrey*, 2009]. The direction of subduction of the downgoing plate varies along the western margin of the Sundaland block being near orthogonal near Java to 60° in the central Sumatra, reducing to 45° in northern Sumatra and becoming almost parallel to the Andaman Island further north. Like the obliquity, the rate of subduction also changes along the western margin of the Sundaland block. It remains nearly 63 mm/yr adjacent to the Java trench, becomes 50 mm/yr near the Nias island, gradually reduces to 45 mm/yr at the NW of Sumatra and becomes 39 mm/yr near the Andaman island [*Chlieh et al.*, 2007; *Cattin et al.*, 2009]. Sparse geodetic data indicate that the rate of convergence lies between 14 mm/yr and 34 mm/yr at the north of 8° [*Gahalaut et al.*, 2006; *Paul et al.*, 2001]. The oblique motion of the oceanic plate leads to the partitioning of slip into two directions: a trench normal component associated with pure thrust faulting and a trench subparallel component influencing the strike-slip dextral movement along the GSF. A series of volcanoes are present along the western boundary of the Sumatra mainland. Co-location of volcanoes with the GSF demonstrates a curvilinear shape. The location of the chain of volcanoes near the GSF indicates that there might be a link between their origins.

[9] The subducting oceanic plate beneath Sumatra has an age variation ranging from 50 to 75 Ma [*Chlieh et al.*, 2007]. More mature oceanic crust (>55 Ma) [*Chlieh et al.*, 2007] and higher dip angles of subducting lithosphere [*Khan and Chakraborty*, 2005] are found toward the north of the subduction zone [*Sdrolias and Müller*, 2006]. The thickness of deposited terrigeneous sediments also increases toward the north from 2 to 6 km [*Chlieh et al.*, 2007]. As a consequence, the depth of the subducting plate below major calc-alkaline volcanoes varies from south to NW of Sumatra, 120–160 km beneath Bali/Java to 100 km beneath northern Sumatra [*Rock et al.*, 1982].

[10] Western offshore Sumatra has experienced several devastating earthquakes from historical periods. Many major events of M_w >8.0 and numerous shorter events of magnitude between 7.2 and 7.9 have been concentrated between 2°N and 7.5°S along the existing islands of the western margin of Sumatra [*Briggs et al.*, 2006; *Hsu et al.*, 2006; *Chlieh et al.*, 2007]. The slip on the megathrust during the 26th December 2004 earthquake was as high as 20 m near offshore northern Sumatra [*Subarya et al.*, 2006]. After 11 years, a region 500 km SW to Banda Aceh was stuck by a major intraplate strike-slip earthquake (Mw ~ 8.6) in 2012 but it did not cause any significant damage.

3. Study Area, Geomorphology and Seismicity

[11] Our study area (Figure 1 and Figure S1 in the auxiliary material) includes northern Sumatra and its immediate offshore which is bordered in the north by the Indian waters, in the east by the Mergui basin, and in the west by the Aceh basin which is a forearc basin associated with the Sumatran subduction process.[1] The Mergui basin is a part of the north Sumatran back arc basin and was developed by the extension of the continental crust of the Malay Peninsula in the Oligocene period [*Curray*, 2005]. In 2005, we acquired bathymetry data offshore Banda Aceh (Figures 1b and 2) which, along with the land topographic data, show that the main GSF bifurcates on Sumatra mainland at 4.93°N, 95.55°E into two distinct fault segments, the Aceh Fault in the south and the Seulimeum Fault in the north, which run almost parallel to each other (NW-SE strike) offshore Banda Aceh. The northern Seulimeum Fault follows the volcanic arc whereas the southern Aceh Fault enters the sea at the southern margin of the Breueh Basin. Further northwest, the Aceh Fault runs through the center of the Breueh Basin expressed by a push-up ridge. The Breueh Basin is narrow, 20 km wide, and lies at 2000 m water depth (Figures 2b and 2c). Its NW-SE strike suggests it was formed by the transtensional Aceh strike-slip fault. In the north it is bounded by the 3.4 km deep, 20 km wide Weh Basin and in the south by the flat-lying Sumatra Platform, which is the offshore extension of the Sumatra continental crust [*Singh et al.*, 2012]. The Weh Basin is bordered by normal faults on either side, is rhomb-shaped, and seems to have been formed by a pull-apart process by the strike-slip Seulimeum Fault in the southeast

[1]Auxiliary materials are available in the HTML. doi:10.1029/2012GC004122.

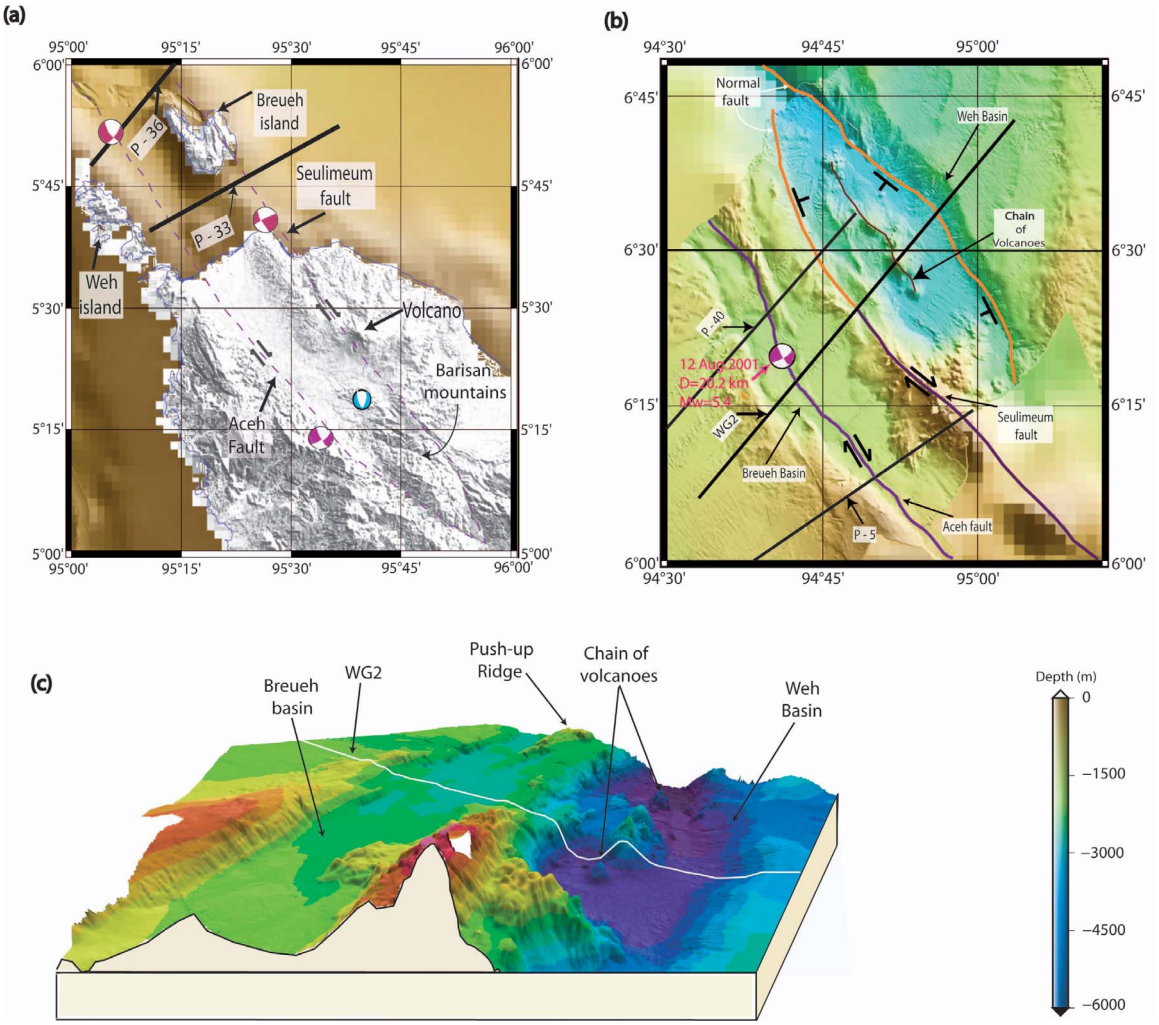

Figure 2. (a) Detailed map of the Banda Aceh region. The Aceh fault and the Seulimeum fault are marked by the dashed line. (b) Detailed map of submarine extension of the Sumatra fault. The two branches (Aceh and Seulimeum) have been marked in purple. The normal extension of the Seulimeum fault is shown in yellow. Black lines indicate seismic profiles. (c) 3D perspective view of different structural features. Push-up ridge inside the Breueh basin and the chain of volcanoes passing through the Weh basin are marked. White line: WG2 profile.

and an unknown fault in the northwest; we do not have high-resolution bathymetry data from the Indian waters. There are at least four volcanoes in the center of the basin (Figure 2), suggesting that the volcanic center has moved northward due to local extension. These volcanoes are mostly elliptical in shape.

[12] Focal mechanisms (from the Harvard CMT catalog), geomorphic expression of faulting on Weh Island and evidence of faulting on previously recorded seismic profiles [*Peter et al.*, 1966; *Weeks et al.*, 1967] suggest that the Seulimeum Fault is active [*Sieh and Natawidjaja*, 2000] and cuts across the Plio-Pleistocene sediments and the active Seulawai Agam volcano. Movement of the Seulimeum Fault has displaced east-west trending sedimentary folds toward the northwest [*Barber and Crow*, 2005].

[13] The seismicity of this area shows a complex deformation pattern (Figure 1b). Southeast of the Aceh-Seulimeum fault junction, there is a cluster of earthquakes with strike-slip focal mechanisms, suggesting that the GSF is active until this junction. Northwest of the Weh Basin, there are several earthquakes aligned in the NW direction with strike-slip focal mechanisms, indicating that this part of the GSF system is active. A burst of seismic activity north of the intersection of the Aceh-Seulimeum faults and the West Andaman Fault exhibits dominantly strike-slip focal mechanisms. However, only

five strike-slip fault earthquakes and one normal fault earthquake have occurred between 5° and 6.9°N along the ~250 km long segment of the GSF system (Figure 1b). There are two possibilities for this low level of seismicity: (a) the bifurcation and segmentation of the GSF system in this area may result in the distributed deformation over a larger area producing only small earthquakes not recorded by global seismological network or (b) this segment of the GSF is either aseismic or is locked and may produce larger earthquakes in the future.

4. Multi Channel Seismic (MCS) Survey and Data Analysis

4.1. Data Collection

[14] The data sets used here were collected from two major seismic expeditions. Single channel seismic reflection data were acquired in 1991–1992 along the western margin of Sumatra [*Malod and Kamal*, 1996]. These data were recorded on paper strips, which were scanned, digitized and converted into SEGY format. In the absence of any velocity information, these data were migrated using a water velocity of 1.5 km/s in order to remove the effect of seafloor scattering. Five profiles traverse the GSF system offshore northern Sumatra. A coincident refraction survey and multichannel seismic (MCS) reflection was carried out in July–August of 2006 using the French (R/V) Marion Dufresne and the Western Geco company's M/V Geco Searcher vessel towing 8260 (~135.35 L) and 10170 (~163.87 L) cubic inch air gun array seismic sources respectively [*Singh et al.*, 2008; *Chauhan et al.*, 2009]. During this survey three profiles were shot over NW offshore Sumatra. Among them only one profile, named the WG2, was shot crossing the subduction front, accretionary prism, Sumatra Platform and back arc. The refraction data were acquired using ocean bottom seismometers spaced at 8.1 km along the WG2 profile. The reflection data were acquired using two streamers: one short streamer with a length of 5.5 km towed at 7.5 m water depth and the second 12-km long streamer towed at 15 m water depth. The short shallow streamer had a notch at 100 Hz and hence has a usable bandwidth of 20–80 Hz providing high-resolution seismic image of the near surface. The long deep streamer had a notch at 50 Hz, i.e., a bandwidth of 8–40 Hz providing low frequency energy essential for deep seismic imaging. The long streamer data were processed by Western Geco using conventional processing techniques for deep seismic imaging [*Singh et al.*, 2008, 2012]. Here we apply advanced analysis techniques to a part of the WG2 MCS data (92 km) around the GSF.

4.2. Multi Channel Refraction Seismic Data Analysis

[15] The estimation of accurate seismic velocities is essential for seismic imaging and interpretation, which can be obtained from both refraction data and reflection data. Since the OBS spacing during the refraction survey along the profile WG2 was 8.1 km, the velocity resolution is on the scale of 10 km laterally and 1–2 km vertically [*Singh et al.*, 2012], which is not sufficient for high-resolution seismic imaging. Since there are not many identifiable reflection arrivals in the MCS data, particularly around the volcano (Figure 5), the reflection data do not provide any information on velocity. However, the long streamer data contain some refracted phases, but these phases arrive only at far offsets and hence do not contain any information on near surface velocity. To overcome these issues, we have downward continued the surface seismic data (both shots and receivers) to the seafloor [*Arnulf et al.*, 2011], which led to the refraction phases arriving close to zero offset up to 12 km that contain detailed information on near surface seismic velocity structure. These first refracted phases were picked and used in the travel time inversion. The details of downward continuation and travel time tomography methods are illustrated in sections S1 and S2, respectively.

4.3. Wide-Angle Multi Channel Seismic Tomographic Results

[16] We tested two different starting models for the inversion: (a) an existing 2D [*Chauhan et al.*, 2009] velocity model that was obtained using (8.1 km OBS spacing) OBS tomographic analysis (Figure 3a), and (b) an average 1D velocity model hung on the seafloor to obtain a 2D velocity model (Figure 3c). The initial χ^2 (root mean square difference between observed and calculated travel time) for the two starting models were ~70 ms and ~100 ms, respectively, suggesting that the model derived using OBS data is closer to the final model.

4.3.1. Inverted Velocity Model

[17] Inverted velocity models produced using two different starting models (Figures 3b and 3d) are very similar, which indicates that the inverted model is a global model for the given travel-time data. Figure 4a shows the velocity anomaly, which is obtained by subtracting the starting velocity model (Figure 3a) from the inverted velocity (Figure 3b).

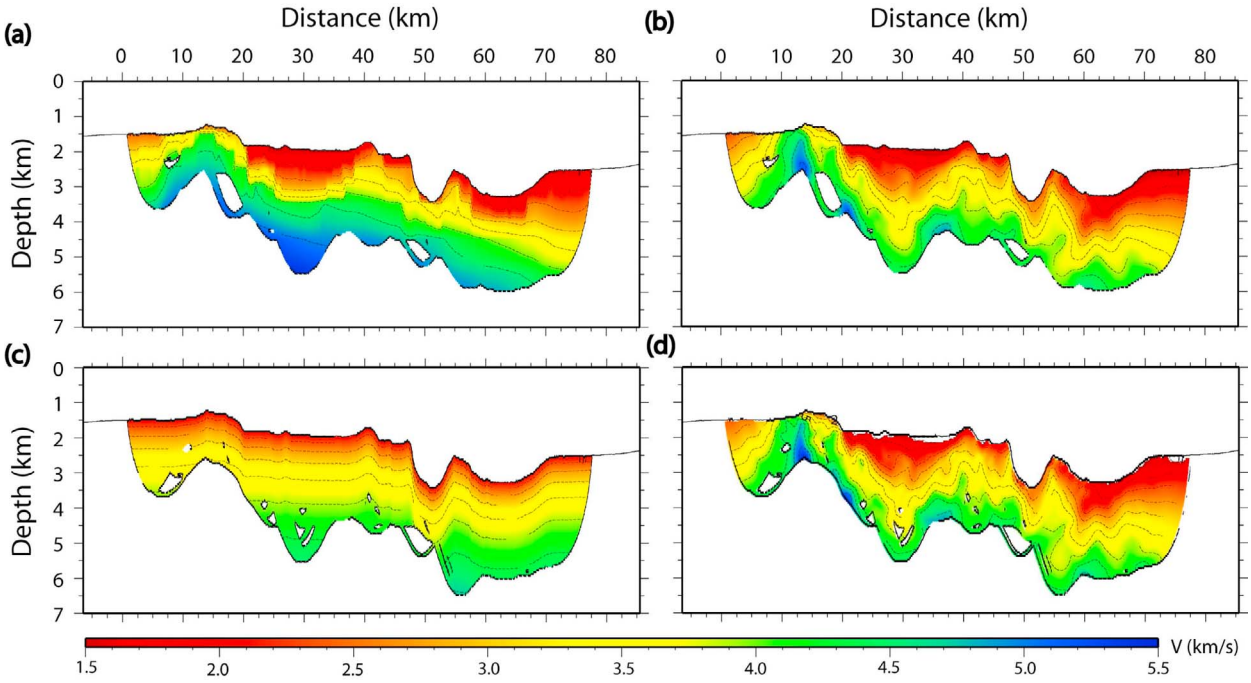

Figure 3. Travel time inversion conducted using two different starting models. (a) The 2D starting model based on OBS tomographic results [*Chauhan et al.*, 2009] and (b) the final inversion result. (c) Starting model obtained by hanging a 1D average velocity profile on the seafloor and (d) corresponding final inversion result.

The ray coverage can be expressed through the derivative weight sum (DWS) plots (Figure 4b), which are derived by summing the columns of the Fréchet derivative matrix [*Scales*, 1987]. Although this plot does not provide actual information on resolution, it does give information about the ray coverage or the sensitivity of a model parameter to the data [*van Avendonk et al.*, 2001].

[18] The ray coverage is significantly high all through the shallow part of the model except at a distance of 12–13 km with respect to 0 km. Since the horizontal velocity gradient varies from the Breueh Basin to the Weh Basin, the ray coverage is not uniform along the profile. Changes in the velocity gradient combined with the irregularities of the bathymetry influence the actual trajectories of the raypaths. Since the bathymetry is comparatively rough over the Weh Basin as compared to the Breueh Basin, the nature of the raypaths changes laterally. We only show the portion of the model that has been sampled by the rays. The maximum depth of ray penetration is 6 km beneath the volcano (Figure 4b).

[19] The very high velocity (>5 km/s) very close to seafloor at around 13 km distance from the 0 km indicates the presence of a crystalline crust (Figure 3),

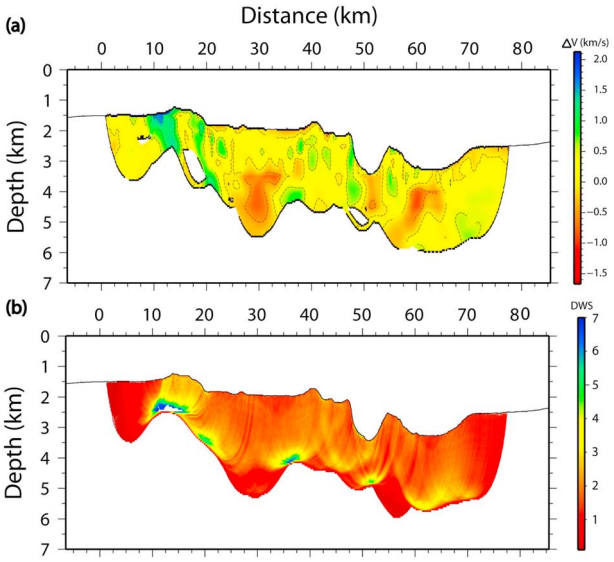

Figure 4. (a) Velocity anomaly: The difference between the OBS tomography derived 2D starting model and the final inversion result. (b) The derivative weight sum (DWS) for the best fit model. The DWS is calculated adding the elements of each column of the Frechet derivative matrix. It is a dimensionless measure of the sensitivity of the data to a model parameter [*van Avendonk et al.*, 1998]. The DWS is plotted in between 0.1 and 7.

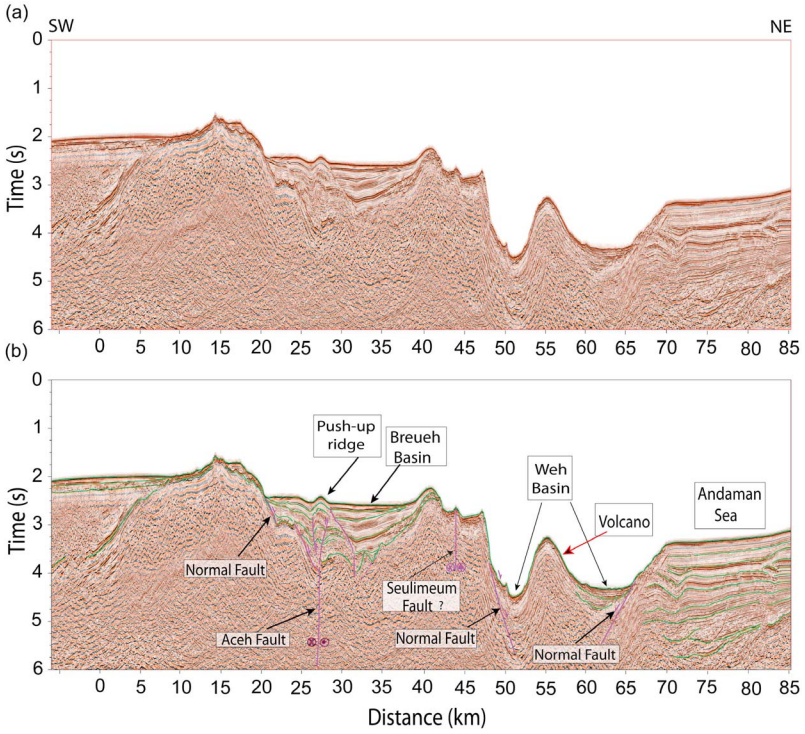

Figure 5. Time migrated seismic image along the profile WG-2: (a) uninterpreted and (b) interpreted. V.E. is 4:1 (at water velocity 1.5 km/sec). The data was processed using a standard processing technique [*Chauhan et al.*, 2009].

which is consistent with the interpretation of the Sumatra Platform being the offshore extension of mainland Sumatra [*Singh et al.*, 2012]. The low velocity at greater depth in the Breueh Basin could be due to the presence of sediments deposited along the transtensional Aceh Fault. Although not well constrained, there seems to be a high velocity beneath the Breueh Basin, suggesting the presence of crystalline basement of continental origin. The northeastern margin of the Breueh Basin is bounded by high-velocity (3.5 km/s) material close to the seafloor, which could be either of volcanic or continental origin. As expected, the volcano is underlain by cone-shaped velocities between 2 to 3.5 km/s, which is consistent with velocities observed beneath the volcanoes (Figure 3b). The basin floor of the Weh Basin has 500–1000 m thick low-velocity material, which could be due to the presence of volcanic debris and/or recent sediments. At the northeast end of the profile, there is a smooth velocity gradient with a thicker low velocity zone in the upper layer, indicating a sedimentary basin type structure expected for the Mergui Basin. The velocity anomaly plot (Figure 4a) contains structures that could be linked to faults observed at the seafloor (Figure 2).

4.4. Seismic Reflection Results

[20] Although we determined a velocity along profile WG2, we do not have any velocity information along five single channel profiles. Therefore, we first interpret all the seismic images in the time domain to get a sense of lateral continuity of the main features imaged on the seismic profiles and their relation with surface morphology.

4.4.1. WG2 Profile

[21] We processed the data from the short streamer to obtain a high-resolution time domain seismic image along profile WG2. The 5.5 km long streamer data were re-sampled to 4 ms, keeping a group interval of 12.5 m and corresponding CMP spacing of 6.25 m. The seismic processing steps were as follows: swell noise attenuation, multiple suppression using iterative Radon filtering, velocity analysis and stacking. Post-stack 2-D Kirchhoff migration was applied using a smooth velocity model [*Singh et al.*, 2008], and a part of the seismic image is shown in Figure 5.

[22] A southwest-dipping reflector is imaged at the southwestern end of the profile (Figure 5), which is overlain by semi-transparent horizontal reflections that have high velocities (Figure 3b), suggesting the

presence of highly compacted sediments. The presence of high velocity underneath this reflector suggests that it could be crystalline basement. The recent sediments in the Breueh Basin represent the low velocity anomaly (Figure 4a) observed using refraction data, and show folding and faulting. The thickness of sediments varies from 0.5 s to 1.5 s. The SW bank of the basin is bounded by a normal fault and a rotated fault block. There is a push-up ridge above the thickest part of the basin (Figure 5b), suggesting a complex deformation pattern. The basement beneath the push-up ridge is faulted (∼at 27 km distance) and has a vertical offset of about 200 ms. This could be the site of the main branch of the strike-slip Aceh Fault. A second basement low-velocity zone (Figure 3b) is observed about 5 km NE of this fault, which could be the position of another branch of the Aceh Fault. The presence of deformed sediments between these two faults with sediments dipping to the NE suggests that it has some thrust component. These faults and sediments above them show a flower structure with deformation observed near the seafloor, suggesting the Aceh branch of the GSF fault is active. The deeper sediments further NE of the second fault dip southwestward, whereas those near the seafloor are nearly flat, suggesting that the deformation is mainly taking place between the SW bounding normal fault and the second fault over a 12.5 km wide zone. The recent sediments SW of this basin are very thin (100 ms) at 1.5 km depth with a flat seafloor without any deformation.

[23] Further NE of the Breueh Basin, there is an 8 km wide deformed zone containing three rotated fault blocks (between 42 km and 50 km distance ranges) without any recent sediment, suggesting the presence of active normal faulting (Figure 5b). No evidence of volcanic material is observed even though the blocks lie along the NW trend of the volcanoes observed on land, suggesting that the volcanic center has shifted north to the center of the Weh Basin. The SW margin of the Weh Basin has a slope of ∼75°, which might have produced by normal faulting with a strike-slip component. A veneer of ∼400 ms thick sediments is present SW of the volcano, where the apex of deposition has shifted northeastward, and is likely to be of volcano-clastic origin. No coherent reflections are observed beneath the volcano. The coherent reflections from sediments in the Weh basin are very thin (up to 400 m), suggesting that this deep basin is recent. The basin is bounded by a basinward dipping fault with a slope of 45°, suggesting this fault should be the antithesis fault of the main fault southwest of the basin (Figure 5b). A thick (2.5 s) sedimentary basin tilting toward the Weh Basin is present, which seems to have undergone some deformation.

4.4.2. Profile 40

[24] Among all the seismic profiles acquired in the study area, this profile is the farthest from WG2 lying 9 km NW of it (Figures 6a and S6a). It is 61 km long traversing the Sumatra Platform at 1700 m water depth and the Breueh Basin, terminating at the SW end of the Weh Basin. The SW flank of the Breueh Basin seems to be bounded by a normal fault with a vertical relief of 0.5 s. The Breueh Basin is about 14 km wide and contains 1.2 s thick sediments. The push-up ridge is present at the center of the basin at 35 km distance from the SW end, indicating the location of the Aceh Fault. In the north, the basin is bounded by a northward dipping fault block separating the two basins. Another tilted fault block is imaged at the end of the NE end of the profile, which can be observed as a 15-km long feature on the bathymetric image, suggesting that active deformation is still taking place along with volcanism in the Weh Basin. This interpretation is reinforced by the presence of onlapping sediments up to 0.5 s dipping to the southwest.

4.4.3. Profile 5

[25] This profile is 12 km SE of WG2 and is 55 km long (Figures 6b and S6b). A 400 ms thick sediment is present on the Sumatra Platform at 1500 m water depth. The SW flank of the Breueh Basin is bounded by a steeply dipping tilted fault block with a vertical relief of 750 m in the southwest and 1000 m in the northeast. At the foot of the fault block, a 5 km wide basin containing a ∼600 ms thick layer of recent sediments resembling a flower structure (Aceh Fault) is present and is bounded by faulted blocks (old sediments) or volcanoes. However, the bathymetry data seem to suggest that this volcanic features rise to 375 m water depth, with a very steep slope in the north resembling faults observed further north. It is possible that the Seulimeum Fault coincides with the volcano or lies north of it.

4.4.4. Profile 2

[26] This profile (Figures 6c and S6c) is the longest of all the Sumenta lines (81 km), and traverses all

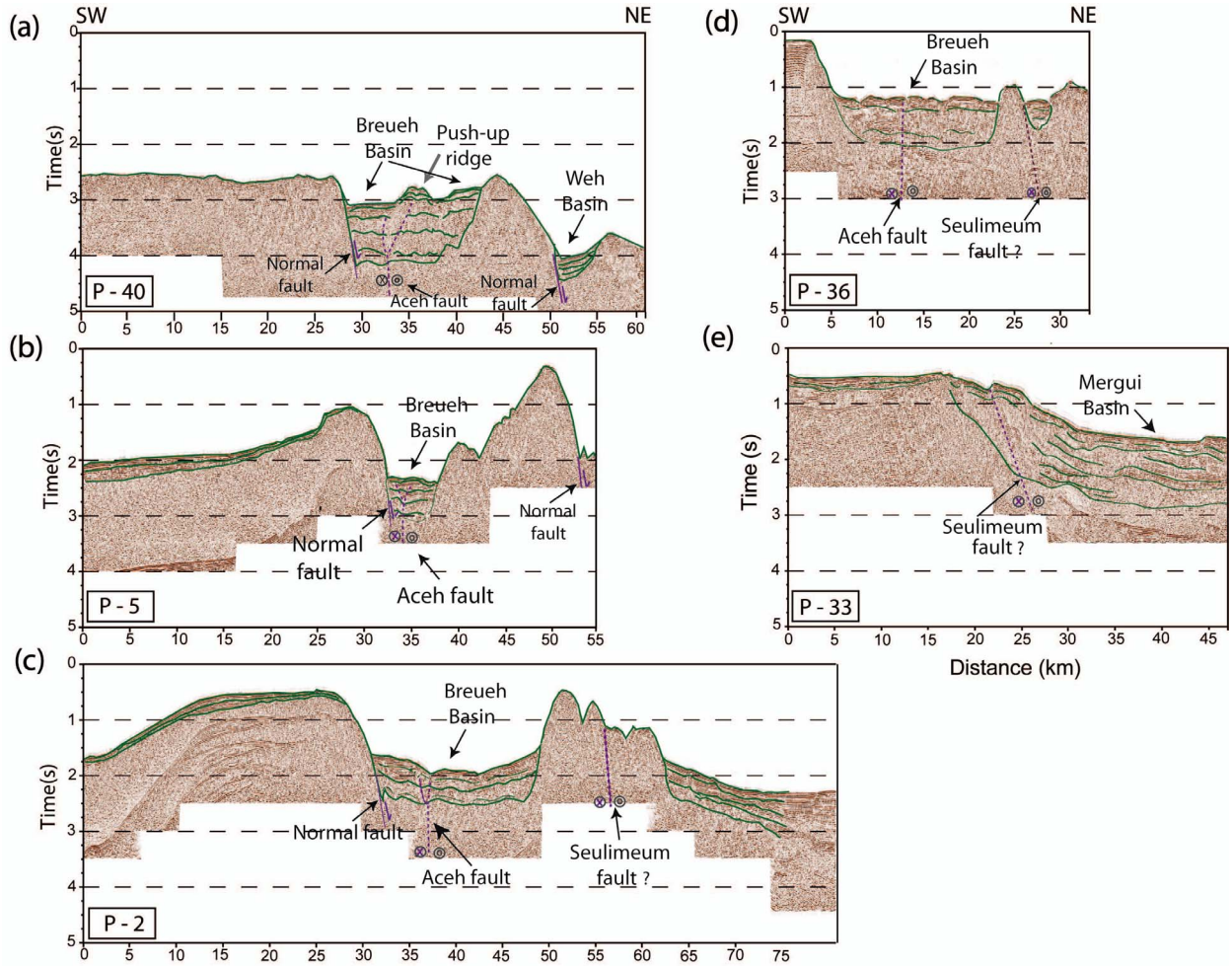

Figure 6. Interpreted single channel seismic reflection profiles from the Sumenta-II *Malod and Kamal* [1992] survey. (a) Profile-40 (P-40), (b) Profile-5 (P-5), (c) Profile-2 (P-2), (d) Profile-36 (P-36) and (e) Profile-33 (P-33).

the features observed on profile WG2. Unfortunately no bathymetry data are available along this profile hence it is difficult to interpret the seismic data alone. However, one can clearly see the tilting of the Sumatra Platform trenchwards with a tilted fault block at the SW boundary of the Breueh Basin and volcanic structures NE to this basin. The Breueh Basin is 23 km wide and 1.5 km deep and holds a 1.0 s thick sedimentary layer. The Aceh Fault passes through the Breueh Basin 37 km from the origin of the profile (Figure 6c). The volcano has three peaks and is aligned with Weh Island, which is of volcanic origin, and is bounded by northeastward tilted sediments that thicken northeastward. It is possible that these sediments belong to the Mergui Basin, similar to those observed at the northeastern end of WG2. Therefore, we suggest that the Weh Basin terminates northwest of Profile 2.

4.4.5. Profile 36

[27] This profile is ~2 km northwest of the Weh Island (Figures 6d and S6d). It is the shortest profile (33 km), but crosses the 21 km wide Breueh Basin. The southwest flank of the Breueh Basin is very steep, and the basin lies at 1000 m depth in the form of a channel as observed on profile WG2. The sediments are presumably disturbed by currents but a depocenter seems to be present at the southwestern end of the basin, which might be the site of the Aceh Fault. A small (3 km wide and 500 ms thick) basin is present between two volcanic-looking features, and might be the site of the Seulimeum Fault (Figure 6d). The topography of Weh Island clearly shows NW-SE trending linear features, cutting through the volcano, suggesting the presence of a fault.

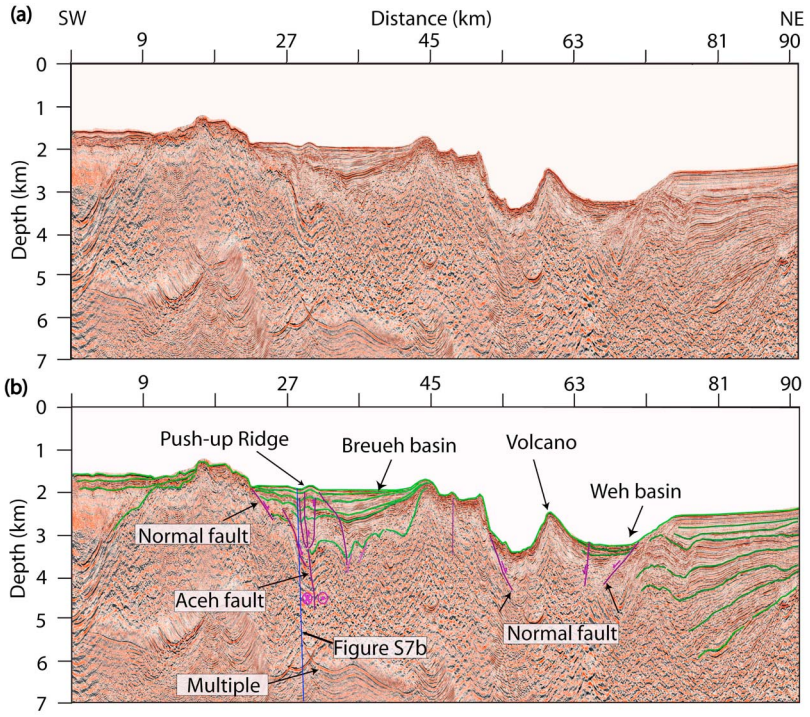

Figure 7. Pre-stack depth migrated seismic image along profile WG-2: (a) uninterpreted and (b) interpreted.

4.4.6. Profile 33

[28] Profile 33 lies between Weh Island and mainland Sumatra, and covers a part of the Breueh Basin and Mergui Basin (Figures 6e and S6e). It is 47 km long and the water depth varies from 375 m in the Breueh Basin to 1275 m in the Mergui Basin. There is a veneer of thin sediments (150 ms) over what looks like old deformed sediments in the Breueh Basin. There are no volcanic features observed near the seafloor northeast of this basin, but a small bathymetric depression is observed that might be a near surface expression of the Seulimeum Fault (Figure 6e). Further NE, thick sediments are present but have poor reflectivity.

4.5. Pre-Stack Depth Migrated Image of the Profile WG2

[29] The methodology for pre-stack depth migration is described in section S3 in the auxiliary material. Figure 7 shows the final pre-stack depth migrated image obtained using the velocity determined from tomography (Figure 3b). The features discussed in section 4.4.1 are clearly observed in the depth image. The Aceh Fault segment of the GSF is clearly observed in the depth section. The two normal faults at the flank of the volcanoes are delineated in the migrated section. The normal faults that were identified in the time section in the Weh Basin are also clearly demarcated in the depth migrated section.

5. Combined Interpretation

[30] The high-resolution bathymetric data, single-channel seismic images, high-resolution tomographic results, pre-stack depth-migrated results and earthquake data are used to correlate the seafloor geomorphic features with the subsurface structures. We merged the depth section of the WG2 image and velocity model with 3D bathymetry to interpret the lateral extent of the main features (Figure 8). The correlation between the seismic-depth image and the velocity model is intriguing, despite tomography providing a smooth velocity model. Although the conformable sediment thickness between the volcano and the Mergui Basin in the Weh Basin is only 300 m, the low velocity zone extends down to 1 km below the seafloor, suggesting that the lower part of this low velocity zone could have been formed by volcanic debris (Figure 8a). The seismic reflection image indicates the presence of steeply dipping faults NE of the volcano, bounding this low velocity zone, which is likely to have been caused by volcanic loading. The vertical velocity gradient map (Figure 8c) suggests that the NE bounding fault

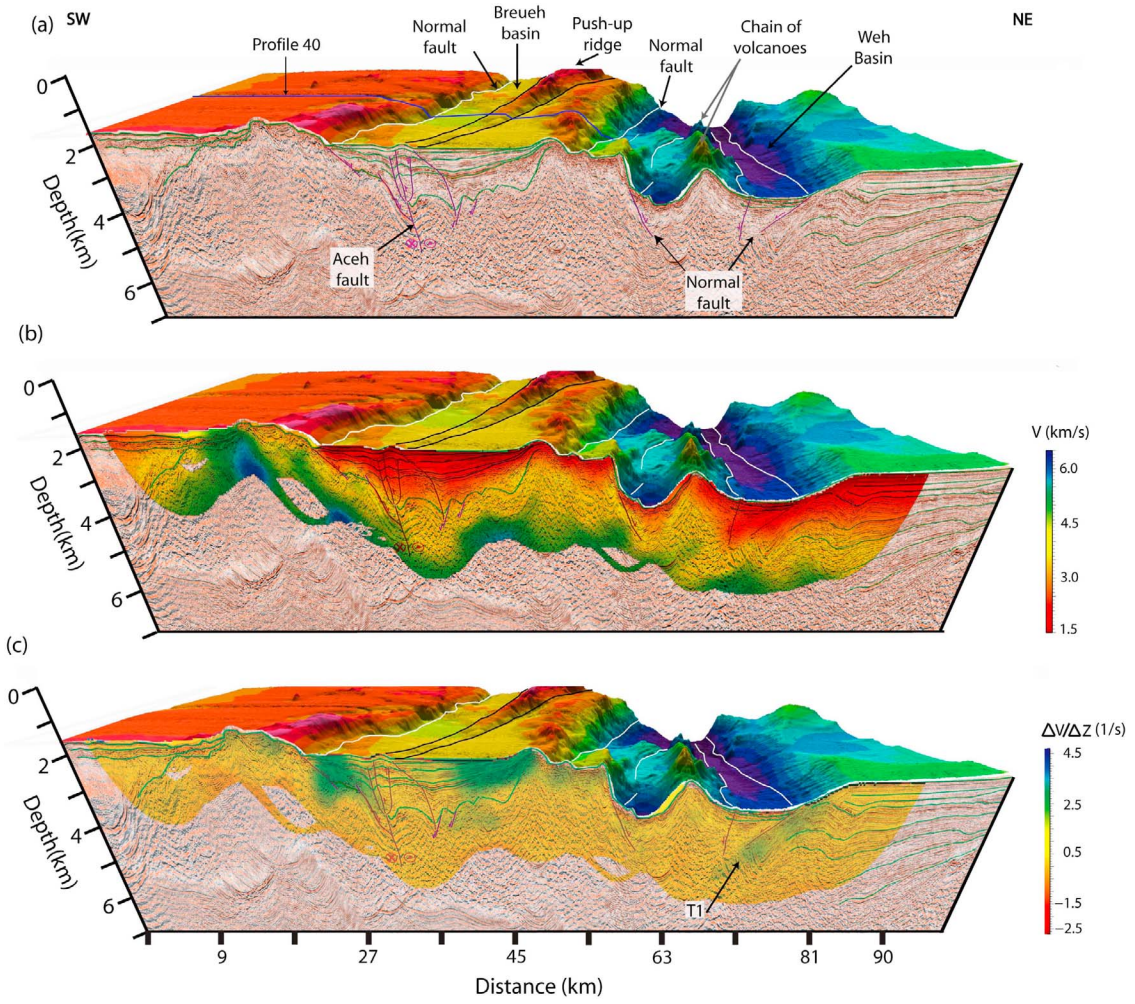

Figure 8. (a) Three-dimensional perspective view of the profile WG2 with bathymetry. The chain of volcanoes is prominent here and several normal faults are shown. Location of profile-40 is also marked. (b) Same as Figure 8a with inverted velocity model superimposed. (c) Same as Figure 8a with the velocity gradient superimposed. The interpreted fault is aligned with the velocity gradient plot marked below the Weh Basin. T1: marks the coincident velocity gradient and the normal fault.

of the Weh Basin lies above a zone with a strong velocity gradient. The southwestern bounding fault of the Weh Basin separates the high velocity crystalline crust in the southwest from the volcanic debris in the northeast. Although the low velocity indicates that the Breueh Basin is symmetric, the seismic reflection image suggests that the Aceh Fault, responsible for the basin formation, lies slightly southwestward.

[31] From bathymetry and seismic images, it is clear that these basins have variable width, depth and thickness of sedimentary layers along the strike of the GSF and volcanic chain. The average width of the Breueh Basin is ~20 km and the water depth varies from 1 km (on profile 36) to 2 km (in profile 40) which implies that the Breueh basin becomes deeper toward the north (Figures 5 and 6). The thickness of accumulated recent sediments varies between 0.5 s and 1.5 s (TWT) (on WG2 profile it is around 3 km) and increases northward (Figure 6).

[32] The push-up ridge seems to grow northwestward (Figure 8a) and may be associated with the vertically dipping Aceh Fault. Although it has been suggested that the Aceh Fault segment is not active north of 5.4°N [*Sieh and Natawidjaja*, 2000] and has not accumulated strain of more than a few mm/yr across the fault [*Genrich et al.*, 2000]. Nonetheless, the presence of strike-slip earthquakes above the Aceh Fault and evidence of positive flower structures (Figure 8) strongly suggest that the offshore extension of the Aceh Fault is still active and maintains its strike-slip nature for ≥135 km NW of Sumatra.

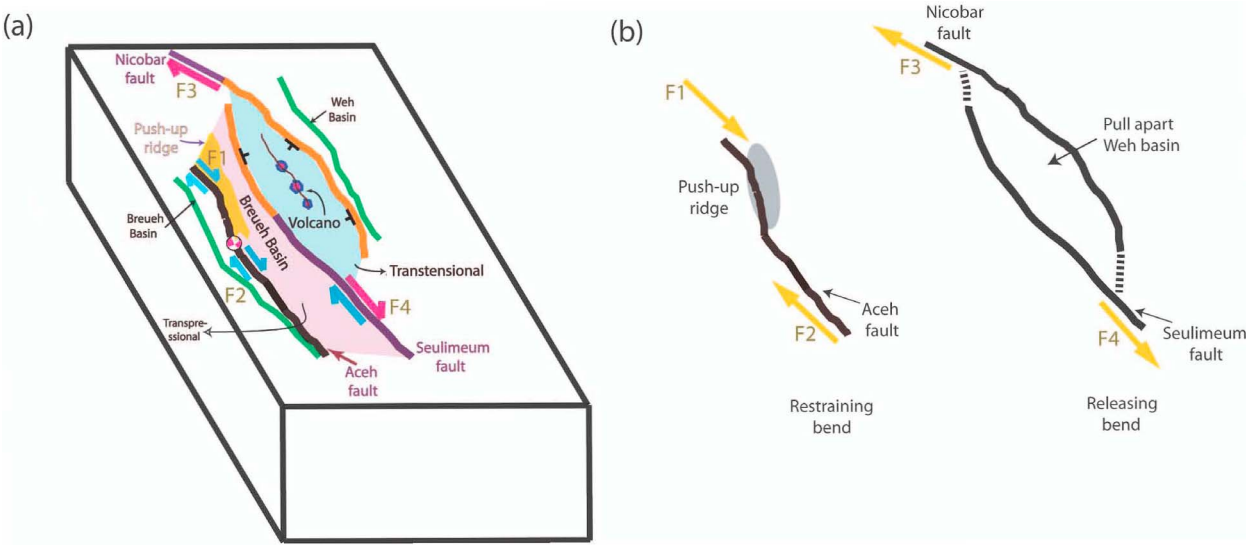

Figure 9. (a) Schematic diagram illustrating the forces (F1, F2, F3 and F4) acting over the Breueh and the Weh basins. Aceh fault, Seulimeum fault and normal faults are represented by black, violet and orange colors respectively. (b) Restraining bend associated with the Aceh fault develops the push-up ridge in the Breueh basin, whereas releasing bends are involved in the development of the pull-apart Weh basin.

[33] The 70-km long and 20-km wide rhomboid-shaped Weh Basin is relatively deep (3.4 km) (Figures 1b and 7b) and is bounded by a steep normal fault to the SW and a relatively shallow dipping normal fault to the NE. The southwestern fault is parallel to the Seulimeum Fault in the SE whereas the NE fault is aligned with the narrow basin observed NW of our study area. These two basin-bounding normal faults could be step-over branches of the Seulimeum Fault, and the basin might have formed by a pull-apart process.

[34] The map view described in Figure 9a clearly shows that the two strands of the GSF, the Seulimeum Fault and Aceh Fault, extend northward. The Seulimeum Fault follows the weak zone created by the chain of volcanoes, whereas the Aceh Fault traverses through a complex transpressive Breueh Basin, which contains flower structures and a push-up ridge at its center. The signature of the compression is further documented by the shallowing of velocity contours within the Breueh Basin. The Seulimeum Fault, a strike-slip fault, terminates near profile 2 and is replaced by two normal faults 5 km apart at the SW flank of the pull-apart Weh Basin. The steep dip (>70°) of these faults suggests that some strike-slip motion might have taken place along them. The NE margin of the volcanic chain is bounded by other normal faults dipping steeply (70°) to the SW, which could be the conjugate of the inner fault observed SW of the volcanoes. The Weh Basin is bounded by a southward shallow (35°) dipping normal fault. All these normal faults seem to merge at the northern end of the Weh basin, which is connected with another strike-slip fault that we call the Nicobar Fault (Figure 1). The volcanoes move northward in the middle of the weak zone at the center of the Weh Basin (Figure 8). The presence of a 0.5 km thick undisturbed sedimentary layer (Figure 7) indicates that the NE part of the Weh Basin is less affected by upper Neogene deformation (considering a sedimentation rate of 4 mm/yr and sedimentary layer velocity of 2 km/sec). The absence of strike-slip events along the offshore Seulimeum Fault segments clearly demarcates the existence of a 200 km seismic gap, which could be a site of a great earthquake if the whole fault segment ruptures simultaneously.

6. Discussion

[35] Here, we have shown that the NW extension of the GSF branches into the Aceh Fault and Seulimeum Fault and that these faults coexist with two submarine basins with distinct morphology. In addition, we have observed submarine volcanoes that are extensions of the volcanic arc observed sub-aerially on Sumatra. Although the geometry and the velocity structures of different parts of these basins are imaged in the seismic studies, more questions need to be addressed to build a comprehensive structural framework over this region. In the following discussion we address the tectonic activity of the Aceh Fault and its close

association with the geometry of the Breueh Basin, the plausible explanations for the anomalous shape and size of the Weh Basin, the correlation between the GSF and the volcanic arc and probable seismic hazards over the northern segment of Sumatra.

6.1. Tectonism in the Breueh Basin

[36] The undulations in the velocity contours of the folded sedimentary layers below the seafloor and the seismic reflection images depict the tectonic activity shaping the basin structures. The presence of the flower structure shows that the Aceh branch of the GSF is strike-slip in nature. Additionally, focal mechanisms of recorded recent earthquake events in the Breueh Basin (Figures 1 and 2b) confirm the idea that the Aceh Fault is active which contradicts suggestions that the Aceh fault is passive offshore northern Sumatra [*Sieh and Natawidjaja*, 2000]. Interestingly, the Seulimeum Fault also maintains its dextral nature until midway along the northern flank of the Breueh Basin. It is obvious that the support for the dextral movement of these fault systems comes from the trench sub-parallel shear component of the oblique subduction of the Indo-Australian plate. Figure 9 illustrates the force system acting on this basin. The combined dextral movement of these faults produces a force system which includes different force components directed toward each other producing a transpressive regime inside the Breueh basin. Additionally, the Aceh fault follows a curvilinear path inside this basin developing a restraining bend, which is presumably responsible for the building up of a push-up ridge within the Breueh Basin (Figures 9a and 9b).

[37] The presence of normal faults on the SW side of the Breueh Basin suggest that it might also have undergone extension (Figure 1b). This produces a complex environment within this basin that makes the kinematics of basin formation difficult to fully understand. Although all the governing forces surrounding this basin cannot be fully described by our data, we infer the coexistence of a compressional force system coupled with an extensional vector field.

6.2. Tectonism in the Weh Basin

[38] The Weh Basin is starkly different from the Breueh Basin due to the presence of a chain of volcanoes, which is clearly visible in the bathymetric data (Figures 2b and 2c). The deepest point of this basin is almost 3.5 km suggesting a special structural and tectonic regime.

[39] Based on our observations it seems that the Weh Basin is associated with the arc of the Sumatra subduction system, but it might have been affected by different extensional forces that are associated with north Sumatran back-arc basins. Different hypotheses have been proposed to explain extensional tectonics linked to a back-arc. Some of these mechanisms are either directly related to the active response to asthenospheric processes (e.g., "mantle diapir") [*Karig*, 1971] or as an indirect response to plate boundary conditions (e.g., "rollback of hinge of subducting slab" [*Molnar and Atwater*, 1978; *Elsasser*, 1971; *Faccenna et al.*, 2001; *Hall et al.*, 2003; *Schellart et al.*, 2003], sea anchoring force [*Scholz and Campos*, 1995]) and upper plate kinematics (e.g., "absolute motion of overlying plate" [*Chase*, 1978; *Carlson et al.*, 1983]). *Sdrolias and Müller* [2006] reported that the presence of older (>55 Ma) subducting plate coupled with the absolute motion of the overlying plate away from the trench may initiate back-arc spreading. In addition to this argument they have added more constraint on the direction of the motion of the subducting oceanic plate with respect to the geologic time scale. They suggested that the motion of the Sunda plate has been bidirectional over the last 70 Ma. Initially it moved toward the trench from 50 Ma to 20 Ma and then turned away from the trench during the last 20 Ma. *Chlieh et al.* [2007] provided additional evidence to support the rotation of the Sumatra plate and postulated that trench retreat has taken place only on the northern part of the Sunda plate during the last 20 Ma and that this process might be the cause of the extension of the Sumatran back-arc. Although we cannot completely rule out the influence of extensional forces associated with the north Sumatran back-arc basin on the Weh basin but, the rhomboid shape of the Weh basin suggests that it was most likely formed by a pull-apart process.

[40] The ratio of length and width of the basin is approximately 3:1. Interestingly, the basin is surrounded by a pair of strike-slip faults with some segments of these faults being taken over by normal faults. In addition, some normal faulting is common inside the basin. The coexistence of extensional structures along with the strike-slip faulting are generally explained by pull-apart models [*Sylvester*, 1988] and if the strike-slip motion is active in the intracontinental plate boundaries then a larger pull-apart process may nucleate forming a releasing bend along the segments of principal displacements of the strike-slip fault zone [*Mann et al.*, 1983]. Therefore, we speculate that the Weh Basin is primarily

affiliated with the pull-apart tectonism. Figure 1 shows the close association of the Nicobar and Seulimeum Faults with the basin. The Nicobar Fault is present at the northwest Weh Basin across the 7°N longitude, whereas the Seulimeum Fault extends up to the midway point of the SW limb of the Weh Basin. The steep dips of the normal faults at the SW margin of the Weh Basin suggest some strike-slip motion is taking place all along these faults. From focal mechanisms it is clear that the nature of these faults is dextral strike-slip, and they are separated from each other by a distance of nearly 50 km. If we consider that these faults are the master faults that may generate transtension during their dextral movement, then this component can lead to the creation of a new space for the basin growth. Growth of such a pull-apart basin is very common on the strike-slip plate boundaries. Similar pull-apart tectonics is observed in the Dead Sea Fault [*Hurwitz et al.*, 2002] and the North Anatolian Fault [*Carton et al.*, 2007]. However, further explanation is required to explain the 3.4 km depth which is fairly deep for pull-apart basins. It has been suggested that the volcanic loading can reorient the stresses in the crust and form a feedback mechanism between the extension of the basin and the volcanic eruption [*van Wyk de Vries and Merle*, 1996; *Waltham et al.*, 2008]. Since the volcanoes are rather small, 1 km high and 4 km wide, it is difficult to imagine that the volcanic loading alone can make a basin so deep. Another possibility is that the Weh Basin is a site of rift initiation leading to seafloor spreading, similar to the Andaman Spreading Center further north, which connects the West Andaman Fault in the south with the Sagaing Fault in the north.

6.3. Relationship Between Volcanism and the Great Sumatra Fault

[41] The relationship between Sumatran volcanic arc and the GSF is not well understood. *Bellier and Sébrier* [1994] propose that the volcanic arc is situated directly above the asthenospheric wedge and the GSF extends vertically to the asthenosphere thereby influencing the geometry of the volcanoes, i.e., there could be a genetic relationship between Sumatra fault and the volcanic arc. On the contrary, *Sieh and Natawidjaja* [2000] suggest that the Sumatra fault zone and the volcanic arc act independently. They found that out of 50 young volcanoes only 9 are within 2 km of the GSF while the rest lie at an average of 10 km from the fault. Since only a fraction of volcanoes is close to the fault,, they suggest that proximity of the volcanoes to the fault is a random coincidence.

[42] Our data show that the chain of volcanoes is situated at the center of the Weh Basin where the principal zone of deformation must lie beneath the volcanoes, supporting the idea of a genetic link between the volcanoes and strike-slip faulting. However, without a geochemical study on rock samples, we cannot fully determine whether a genetic relationship exists between the volcanic arc and strike-slip faulting.

[43] Our results can be interpreted in the light of the available studies and evidence collected in other geological studies. *Katili* [1975] postulates that the dip and the position of the subduction zone, which extends from Sumatra to Timor, has changed from Permian to Plio-Pleistocene. They also suggest that the Paleo-locations of the magnetic arc have also migrated in concert with the location and the dip of the subducting plate. *Curray* [2005] suggests that the Sumatra fault system formed between 15 Ma and 4 Ma and bifurcated into the Aceh and Seulimeum segments 4 Ma ago. Therefore, it can be inferred that the formation of the volcanic arc in Sumatra took place before the development of the GSF. It is possible that the volcanism in some locations might have been partially affected by tectonism linked to the Sumatran fault system, however the generation of the volcanic arc is mainly caused by the dehydration of the subducting oceanic slab beneath the overlying Sunda microplate [*Harland*, 1971]. The presence of the volcanic arc may be less influenced by the GSF and instead more affected by the shape of the subducting plate and the physiochemical processes associated with it.

6.4. Seismic Risk

[44] Soon after the disastrous earthquake of 2004, *McCloskey et al.* [2005] suggested that the Coulomb stress at the offshore extension of the Great Sumatra Fault had increased significantly, and they predicted that a significant strike-slip earthquake event should follow, but instead a great megathrust earthquake occurred at 150 km SE of the 2004 epicenter on March 28, 2005. *Cattin et al.* [2009] reported that the cumulative occurrence of 2004 and 2005 earthquake events increased the Coulomb stress by an order of 20 bars offshore of northern Sumatra which has remained seismically quiet for the last 170 years.

[45] The pull-apart basin situated immediately north of Sumatra is surrounded by strike-slip and normal faults, but it lies in a zone where seismicity is significantly less. There is a step-over of 50 km along the basin (Figure 2b). It is true that the pull-apart regions are normally devoid of big earthquakes due

to the presence of reduced interplate friction producing events M <5 [*Segall and Polland*, 1980] whereas slip parallel fault segments produce frequent events of 6.5 < M < 7.5. However, the Aceh Fault is straight for about 200 km and may generate an infrequent but large M ≥8.0 earthquake [*Scholz*, 1977]. Although the rate of convergence decreases northward [*Paul et al.*, 2001; *Gahalaut et al.*, 2006] the slip rate along the GSF falls in a range between 11 and 28 mm/yr in northern Sumatra [*Natawidjaja and Sieh*, 1994; *Genrich et al.*, 2000; *Prawirodirdjo et al.*, 2000]. If a part of this slip is taken along the Aceh Fault, the accumulation of stress over the last 170 years could be quite large and the partial release of this stress or the complete ruptures of the plate boundary may produce a large damaging earthquake offshore Sumatra. It is obvious that the magnitude of the released energy will depend on the nature of interplate locking and different physical properties like pressure, temperature, pore fluids, mineral phase, fault plane roughness and so on along the existing faults [*Byrne et al.*, 1988; *Hyndman et al.*, 1995; *Lay and Bilek*, 2007]. Nonetheless, we can estimate the magnitude of a potential earthquake based on our observations and available information in the literature.

[46] To do so, we use the seismic moment scaling-law method [*Kanamori*, 1983]. Based on the shear modulus (μ) = 3 × 10^{10} N/m^2, length of a fault segment (L), height of a fault segment (H) = 28.5 km (estimated from focal mechanisms) and displacement of fault segment (D) = 2 m (considering the average slip rate of 20 mm/yr and the recurrence interval of 170 years) we can estimate the magnitude of the maximum intensity expected for an earthquake on these segments. We have estimated results for the different segments. If the onshore segment (L = 70 km) ruptures then it can produce an event of M = 7.3 whereas the slipping of the offshore segment (L = 130 km) may generate an earthquake of M = 7.5. On the other hand, the failure of the whole intact seismic gap (L = 200 km) may release a vast amount of energy producing an earthquake of M = 7.6 magnitude.

7. Conclusions

[47] On the basis of bathymetric maps, multi channel reflection and refraction seismic analysis and earthquake data, the following conclusions are made:

[48] (1) The northern branch of the GSF, the Seulimeum Fault, traverses almost 110 km NW maintaining its dextral nature. Further NW, there is a step-over of about 50 km leading to the formation of the pull-apart Weh Basin, which is bounded by a set of four normal faults. The southern strand of the GSF, the Aceh Fault, is a strike-slip fault and extends up to 200 km offshore north of Banda Aceh. Both faults seem to be active.

[49] (2) Two basins of NW orientation are present offshore northern Sumatra. The southern basin (Breueh basin) contains evidence of compressive structure such as a push up ridge, and appears to be formed by a complex extension and compression along the Aceh Fault. The rhomboid-shaped Weh basin is deep (3.4 km deep) and seems to have been formed by a combination of pull-apart and rifting process. A chain of volcanoes passes through the center of Weh Basin, ∼15 km north of the volcanoes on land, and might represent the offshore extension of the volcanic arc.

[50] (3) The zone immediately offshore of NW Sumatra appears to be seismically locked. The northern branch of the GSF, Seulimeum Fault, is segmented into a strike-slip, pull-apart system, and hence is likely to produce smaller earthquakes. However, the southern branch, Aceh Fault, is straight for >200 km and may produce an earthquake of up to 7.6 magnitude. Therefore, this risk should be accounted for in any mitigation plan of earthquake and tsunami risk in this region.

Acknowledgments

[51] We are highly grateful to Western Geco for funding the acquisition of a seismic reflection survey and processing of the data. We are also thankful to Jacques Malod for supplying the single channel seismic data. We are grateful to A. Harding, N. Bangs, H. Carton and A. Arnulf for their technical support. We are thankful to J. Resing and J. Martin for editing the manuscript and grateful to L. McNeil and reviewer 1 for detailed revision and valuable comments. This is IPG Paris contribution 3346.

References

Arnulf, A., A. J. Harding, S. C. Singh, G. M. Kent, and W. Crawford (2011), Strong seismic heterogeneity in layer 2A near hydrothermal vents at the Mid-Atlantic ridge, *Geophys. Res. Lett.*, *38*, L13320, doi:10.1029/2011GL047753.

Barber, A. J., and M. J. Crow (2005), Structure and structural history, in *Sumatra Geology, Resources and Tectonic Evolution*, edited by A. J. Barber, M. J. Crow, and J. S. Milsom, *Mem. Geol. Soc.*, *31*, 175–233.

Bellier, O., and M. Sébrier (1994), Relationship between tectonism and volcanism along the Great Sumatran fault zone deduced by SPOT image analyses, *Tectonophysics*, *233*, 215–231, doi:10.1016/0040-1951(94)90242-9.

Briggs, R. W., et al. (2006), Deformation and slip along the Sunda Megathrust in the great 2005 Nias-Simelue earthquake, *Science*, *311*, 1897–1901, doi:10.1126/science.1122602.

Byrne, D. E., D. M. Davis, and L. R. Sykes (1988), Loci and maximum size of thrust earthquakes and the mechanics of the shallow region of subduction zones, *Tectonics*, *7*, 833–857, doi:10.1029/TC007i004p00833.

Cameron, N. R., C. G. Clarke, D. T. Aldiss, J. A. Aspden, and A. Djunuddin (1980), The geological evolution of northern Sumatra, paper presented at 9th Annual Convention, Indonesian Pet. Assoc., Jakarta.

Carlson, R. L., T. W. C. Hilde, and S. Uyeda (1983), The driving mechanism of plate tectonics: Relation to age of lithosphere at trenches, *Geophys. Res. Lett.*, *10*, 297–300, doi:10.1029/GL010i004p00297.

Carton, H., et al. (2007), Seismic imaging of the three dimensional architecture of the Cinarcik basin along the North Anatonian fault, *J. Geophys. Res.*, *112*, B06101, doi:10.1029/2006JB004548.

Cattin, R., N. Chamot-Rooke, M. Pubellier, A. Rabaute, M. Delescluse, C. Vigny, L. Fleitout, and P. Dubernet (2009), Stress change and effective friction coefficient along the Sumatra-Andaman-Sagaing fault system after the 26 December 2004 (M_w = 9.2) and the 28 March 2005 (M_w = 8.7) earthquakes, *Geochem. Geophys. Geosyst.*, *10*, Q03011, doi:10.1029/2008GC002167.

Chase, C. G. (1978), Extension behind island arcs and motions relative to hotspots, *J. Geophys. Res.*, *83*, 5385–5387, doi:10.1029/JB083iB11p05385.

Chauhan, A. P. S., S. C. Singh, N. D. Hananto, H. Carton, F. Klingelhoefer, J. X. Dessa, H. Permana, N. J. White, D. Graindorge, and the Sumatra OBS Scientific Team (2009), Seismic imaging of forearc backthrusts at northern Sumatra subduction zone, *Geophys. J. Int.*, *179*, 1772–1780, doi:10.1111/j.1365-246X.2009.04378.x.

Chlieh, M., et al. (2007), Coseismic slip and aftershock of the great M-w 9.15 Sumatra-Andaman earthquake of 2004, *Bull. Seismol. Soc. Am.*, *97*, S152–S173, doi:10.1785/0120050631.

Clure, J. (2005), Fuel resources: Oil and gas, in *Sumatra Geology, Resources and Tectonic Evolution*, edited by A. J. Barber, M. J. Crow, and J. S. Milsom, *Mem. Geol. Soc.*, *31*, 131–141.

Crow, M. J. (2005), Tertiary volcanicity, in *Sumatra Geology, Resources and Tectonic Evolution*, edited by A. J., Barber, M. J. Crow and J. S. Milsom, *Mem. Geol. Soc.*, *31*, 98–119.

Curray, J. R. (2005), Tectonics and history of Andaman Sea region, *J. Asian Earth Sci.*, *25*, 187–232, doi:10.1016/j.jseaes.2004.09.001.

Dewey, J. F. (1980), Episodicity, sequence and style at convergent plate boundaries, in *The Continental Crust and Its Mineral Deposits*, *Geol. Assoc. Can. Spec. Pap.*, *20*, 553–573.

Elsasser, W. M. (1971), Seafloor spreading as thermal convection, *J. Geophys. Res.*, *76*, 1101–1112, doi:10.1029/JB076i005p01101.

Faccenna, C., F. Funicieollo, D. Giardini, and P. Lucente (2001), Episodic back-arc extension during restricted mantle convection in the central Mediterranean, *Earth Planet. Sci. Lett.*, *187*, 105–116, doi:10.1016/S0012-821X(01)00280-1.

Fitch, T. J. (1972), Plate convergence, transcurrent faults, and initial deformation adjacent to southeast Asia and the western Pacific, *J. Geophys. Res.*, *77*, 4432–4460, doi:10.1029/JB077i023p04432.

Gahalaut, V. K., B. Nagarajan, J. K. Catherine, and S. Kumar (2006), Constraints on 2004 Sumatra-Andaman earthquake rupture from GPS measurements in Andaman-Nicobar Islands, *Earth Planet. Sci. Lett.*, *242*, 365–374, doi:10.1016/j.epsl.2005.11.051.

Gasparon, M. (2005), Quaternary volcanicity, in *Sumatra Geology, Resources and Tectonic Evolution*, edited by A. J. Barber, M. J. Crow, and J. S. Milsom, *Mem. Geol. Soc.*, *31*, 120–130.

Genrich, J. F., Y. Bock, R. McCaffrey, L. Prawirodirdjo, C. W. Stevens, S. S. S. Puntodewo, C. Subarya, and S. Wdowinski (2000), Distribution of slip at the northern Sumatran fault system, *J. Geophys. Res.*, *105*(B12), 28,327–28,341, doi:10.1029/2000JB900158.

Hall, C. E., M. Gurnis, M. Sdrolias, L. L. Lavier, and R. D. Müller (2003), Catastrophic initiation of subduction following forced convergence across fracture zones, *Earth Planet. Sci. Lett.*, *212*, 15–30, doi:10.1016/S0012-821X(03)00242-5.

Hamilton, W. (1979), Tectonics of the Indonesian region, *U.S. Geol. Surv. Prof. Pap.*, *1078*, 345 pp.

Harland, W. B. (1971), Tectonic transpression in Caledonian Spitsbergen, *Geol. Mag.*, *108*, 27–42, doi:10.1017/S0016756800050937.

Hsu, J. Y., M. Simons, J. P. Avouac, K. Sieh, J. Galetzka, M. Chlieh, Y. Bock, D. H. Natawidjaja, and L. Prawirodirdjo (2006), Frictional afterslip following the Mw 8.7, 2005 Nias Simeulue earthquake, Sumatra, *Science*, *312*, 1921–1926, doi:10.1126/science.1126960.

Hurwitz, S., Z. Gurfunkel, Y. Ben-Gai, M. Reznikov, Y. Rotstein, and H. Gvirtzman (2002), The tectonic framework of a complex pull apart basin: Seismic reflection observations in the sea Galilee, Dead sea transform, *Tectonophysics*, *359*, 289–306, doi:10.1016/S0040-1951(02)00516-4.

Hyndman, R. D., K. Wang, and M. Yamano (1995), Thermal constraints on the seismogenic portion of the southwestern Japan subduction thrust, *J. Geophys. Res.*, *100*, 15,373–15,392, doi:10.1029/95JB00153.

Jarrard, R. D. (1986), Relations among subduction parameters, *Rev. Geophys.*, *24*, 217–284, doi:10.1029/RG024i002p00217.

Kanamori, H. (1983), Magnitude scale and quantification of earthquakes, *Tectonophysics*, *93*, 185–199, doi:10.1016/0040-1951(83)90273-1.

Karig, D. E. (1971), Origin and development of marginal basins in the western Pacific, *J. Geophys. Res.*, *76*, 2542–2561, doi:10.1029/JB076i011p02542.

Katili, J. A. (1975), Volcanism and plate tectonics in the Indonesian island arcs, *Tectonophysics*, *26*, 165–188, doi:10.1016/0040-1951(75)90088-8.

Khan, P. K., and P. P. Chakraborty (2005), Two-phase opening of Andaman Sea: a new seismotectonic insight, *Earth Planet Sci. Lett.*, *229*, 259–271.

Konca, A. O., et al. (2008), Partial rupture of a locked patch of the Sumatra megathrust during the 2007 earthquake sequence, *Nature*, *456*, 631–635, doi:10.1038/nature07572.

Lay, T., and S. Bilek (2007), Anomalous earthquake ruptures at shallow depths on subduction zone megathrusts, in *The Seismogenic Zone of Subduction Thrust Fault*, edited by T. H. Dixon and J. C. Moore, pp. 476–511, Columbia Univ. Press, New York.

Macpherson, C. G., and R. Hall (1999), Tectonic controls of geochemical evolution in arc magmatism in SE Asia, in *Proceedings of the PACRIM 99 Congress*, *Publ. Ser.*, vol. 4/99, 359–368, Aust. Inst. of Mining and Metall., Carlton South, Vic., Australia.

Malod, J. A., and B. M. Kamal (1996), The Sumatra margin: Oblique subduction and lateral displacement of the accretionary prism, *Geol. Soc. Spec. Publ.*, *106*(1), 19–28, doi:10.1144/GSL.SP.1996.106.01.03.

Mann, P., M. R. Hempton, D. C. Bradley, and K. Burke (1983), Development of pull-apart basins, *J. Geol.*, *91*, 529–554, doi:10.1086/628803.

McCaffrey, R. (1992), Oblique plate convergence, slip vectors, and forearc deformation, *J. Geophys. Res.*, *97*(B6), 8905–8915, doi:10.1029/92JB00483.

McCaffrey, R. (2009), The tectonic framework of the Sumatra subduction zone, *Annu. Rev. Earth Planet. Sci.*, *37*, 345–366, doi:10.1146/annurev.earth.031208.100212.

McCloskey, J., S. S. Nalbant, and S. Steacy (2005), Earthquake risk from co-seismic stress, *Nature*, *434*, 291.

Molnar, P., and T. Atwater (1978), Interarc spreading and cordilleran tectonics as alternatives related to the age of subducted oceanic lithosphere, *Earth Planet. Sci. Lett.*, *41*, 330–340, doi:10.1016/0012-821X(78)90187-5.

Natawidjaja, D. H., and K. Sieh (1994), Slip rate along the Sumatran transcurrent fault and its tectonic significance, paper presented at Conference on Tectonic Evolution of Southeast Asia, Geol. Soc., London, 7–8 Dec.

Newcomb, K. R., and W. R. McCann (1987), Seismic history and seismotectonics of the Sunda arc, *J. Geophys. Res.*, *92*, 421–439, doi:10.1029/JB092iB01p00421.

Paul, J., et al. (2001), The motion and active deformation of India, *Geophys. Res. Lett.*, *28*, 647–650, doi:10.1029/2000GL011832.

Peter, G., L. A. Weeks, and R. E. Burns (1966), A reconnaissance geophysical survey in Andaman Sea and across the Andaman-Nicobar Island arc, *J. Geophys. Res.*, *71*, 495–509, doi:10.1029/JZ071i002p00495.

Prawirodirdjo, L., Y. Bock, J. Genrich, S. Puntodewo, J. Rais, C. Subarya, and S. Sutisna (2000), One century of tectonic deformation along the Sumatran fault from triangulation and Global Positioning System surveys, *J. Geophys. Res.*, *105*(B12), 28,343–28,361, doi:10.1029/2000JB900150.

Rock, N. M. S., H. H. Syah, A. E. Davis, D. Hutchison, M. T. Styles, and R. Lena (1982), Permian to recent volcanism in northern Sumatra, Indonesia: A preliminary study of its distribution, chemistry, and peculiarities, *Bull. Volcanol.*, *45*, 127–152.

Scales, J. A. (1987), Tomographic inversion via the conjugate inversion method, *Geophysics*, *52*, 179–185, doi:10.1190/1.1442293.

Schellart, W. P., M. N. Jessel, and G. S. Lister (2003), Asymmetric deformation in the backarc region of the Kuril Arc, northwest Pacific: New insight from analog modeling, *Tectonics*, *22*(5), 1047, doi:10.1029/2002TC001473.

Scholz, C. H. (1977), Transform fault systems of California and New Zealand: Similarities in their tectonic and seismic styles, *J. Geol. Soc.*, *133*, 215–228, doi:10.1144/gsjgs.133.3.0215.

Scholz, C. H., and J. Campos (1995), On the mechanism of seismic decoupling and backarc spreading at subduction zones, *J. Geophys. Res.*, *100*, 22,103–22,115, doi:10.1029/95JB01869.

Sdrolias, M., and R. D. Müller (2006), Controls on back-arc basin formation, *Geochem. Geophys. Geosyst.*, *7*, Q04016, doi:10.1029/2005GC001090.

Segall, P., and D. D. Polland (1980), Mechanics of discontinuous faults, *J. Geophys. Res.*, *85*, 4337–4350, doi:10.1029/JB085iB08p04337.

Sieh, K., and D. Natawidjaja (2000), Neotectonic of the Sumatran fault Indonesia, *J. Geophys. Res.*, *105*, 28,295–28,326, doi:10.1029/2000JB900120.

Sieh, K., D. H. Natawidjaja, A. J. Meltzner, C. C. Shen, H. Cheng, K. Li, B. W. Suwargadi, J. Galetzka, B. Philibosian, and R. L. Edwards (2008), Earthquake supercycles inferred from sea-level changes recorded in the corals of West-Sumatra, *Science*, *322*, 1674–1678, doi:10.1126/science.1163589.

Singh, S. C., et al. (2008), Seismic evidences for broken oceanic crust in the 2004 Sumatra earthquake epicentral region, *Nat. Geosci.*, *1*(11), 777–781, doi:10.1038/ngeo336.

Singh, S. C., A. P. S. Chauhan, A. J. Calvert, N. D. Hananto, D. Ghosal, A. Rai, and H. Carton (2012), Sesmic evidence of bending and unbending of subducting oceanic crust and the presence of mantle megathrust in the 2004 Great earthquake rupture zone, *Earth Planet. Sci. Lett.*, *321–322*, 166–176, doi:10.1016/j.epsl.2012.01.012.

Sleep, N. H., and M. N. Toksoz (1971), Evolution of marginal seas, *Nature*, *233*, 548–550, doi:10.1038/233548a0.

Soetadi, R., and Soekarman (1964), Preliminary notes on the Atjeh earthquake of April 2 1964, *Geophys. Notes, 3*, pp. 1–6, Dorektorat Meteorol. dan Geofisk, Jakarta.

Subarya, C., M. Chlieh, L. Prawirodirdjo, J. P. Avouac, Y. Bock, K. Sieh, A. J. Meltzner, D. H. Natawidjaja, and R. McCaffrey (2006), Plate-boundary deformation associated with the great Sumatra–Andaman earthquake, *Nature*, *440*, 46–51, doi:10.1038/nature04522.

Sylvester, A. G. (1988), Strike-slip faults, *Geol. Soc. Am. Bull.*, *100*, 1666–1703, doi:10.1130/0016-7606(1988)100<1666:SSF>2.3.CO;2.

van Avendonk, H. J. A., A. J. Harding, J. A. Orcutt, and J. S. McClain (1998), A two-dimensional tomographic study of the Clipperton transform fault, *J. Geophys. Res.*, *103*, 17,885–17,899, doi:10.1029/98JB00904.

van Avendonk, H. J. A., A. J. Harding, J. A. Orcutt, and J. S. McClain (2001), Contrast in crustal structure in across the Clipperton transform fault from travel time tomography, *J. Geophys. Res.*, *106*, 10,961–10,981, doi:10.1029/2000JB900459.

van Bemmelen, R. W. (1949),*The Geology of Indonesia*, Martinus Nijhoff, The Hague, Netharlands.

van Wyk de Vries, B., and O. Merle (1996), The effect of volcanic constructs on rift fault patterns, *Geology*, *24*, 643–646, doi:10.1130/0091-7613(1996)024<0643:TEOVCO>2.3.CO;2.

Waltham, D., R. Hall, H. R. Smyth, and C. J. Ebinger (2008), Basin formation by volcanic arc loading, in *Formation and Applications of the Sedimentary record in Arc Collision Zones*, edited by A. E. Draut, P. D. Clift, and D. W. Scholl, *Spec. Pap. Geol. Soc. Am.*, *436*, 11–26, doi:10.1130/2008.2436(02).

Weeks, L. A., R. N. Harbison, and G. Peter (1967), Island arc system in the Andaman Sea, *Am. Assoc. Pet. Geol. Bull.*, *51*, 1803–1815.